

# Simulation of the interband s-d and intraband s-s electron-phonon contributions to the temperature dependence of the electrical resistivity in Fe/Cr multilayers

B.G. Almeida

Dep. Física Univ. Minho, Campus de Gualtar, 4700 Braga, Portugal

V.S. Amaral, J.B. Sousa

IFIMUP, Dep. Física, Fac. Ciências, Univ. Porto, P-4150 Porto, Portugal

R. Colino, I.K. Schuller

Physics Department, Univ. California-San Diego, La Jolla, CA 92093-0319, USA

V.V. Moschalkov and Y. Bruynseraede

Lab. Vaste-Stoffysika en Magnetisme, Katholieke Univ. Leuven, B-3001 Leuven, Belgium

High-resolution electrical resistivity ( $\rho$ ,  $d\rho/dT$ ) measurements were performed in three series of  $[\text{Fe}_{30}\text{ÅCr}_{t}\text{Å}]$  multilayers in the temperature range 15-300K, with an applied magnetic saturation field (7.5kOe). The samples were deposited by MBE on MgO substrates and by sputtering on MgO and Si substrates. For  $T < 50\text{K}$  the ideal resistivity follows  $\rho_i = \beta T^3$  indicating the dominance of phonon assisted interband s-d scattering in this temperature range. For  $T > 150\text{K}$  the resistivity attains the classical regime with  $\rho \propto T$ . To simulate the observed  $\rho_i(T)$  we have used a model that takes into account intraband s-s and interband s-d electron-phonon scattering, written as  $\rho_{sd} = A \times f_1(T)$  and  $\rho_{ss} = B \times f_2(T)$  where  $f_1$  and  $f_2$  are functions only of the temperature, A and B are sample dependent constants and  $\rho_i = \rho_{sd} + \rho_{ss}$ . The model predicts that  $\rho_i \propto T^3$  at low temperatures and  $\rho_i \propto T$  at high temperatures as observed in our multilayers. The experimental curves of  $\rho_i$  and  $d\rho/dT$  are well reproduced in the whole temperature range (15-300K) and from the fits to these curves A and B are determined for each sample. By plotting B versus A we find that each point from all the multilayers falls in a straight line indicating that B is proportional to A. The simulated resistivity thus predicts that  $\rho_i = \beta f(T)$  where  $f(T) = \alpha_1 \times f_1(T) + \alpha_2 \times f_2(T)$  is a function only of the temperature, as observed experimentally.

In recent years much progress has been made in understanding giant magnetoresistance (GMR) and its related phenomena [1]. One of the important aspects of GMR is its temperature dependence. A careful study of the temperature dependence of GMR as well of the underlying electrical resistivity are not only important in understanding its mechanism but also useful regarding realistic applications. In order to deepen our understanding of this problem we have performed a detailed comparative study of the temperature dependence of the electrical resistivity ( $\rho$ ) and its temperature derivative ( $d\rho/dT$ ) on three sets of  $[\text{Fe}_{30\text{\AA}}/\text{Cr}_{t\text{\AA}}]\times 10$  multilayers deposited by different techniques (MBE, Sputtering) over different substrates (MgO and Si). Our objective is to identify dominant electron scattering mechanisms by using detailed measurements of the temperature derivative of the electrical resistivity, and model their T behavior adequately.

The samples were deposited by sputtering over MgO (100) and Si (100) substrates, with Cr-layer thicknesses in the range  $10\text{\AA}$ - $50\text{\AA}$ . Details of the deposition technique were reported elsewhere [2].

The electrical resistivity measurements were performed in the temperature range 15-300K using the standard four probe technique. Absolute values were obtained with the Van der Pauw method.

Figure 1a) and 1b) shows the temperature dependence of the ideal electrical resistivity  $\rho_i = \rho - \rho_0$  ( $\rho_0$  is the residual resistivity) in the temperature range  $15 < T < 300\text{K}$ , for the sputtered sets of samples. Also shown is the corresponding  $d\rho/dT$  temperature dependence in the same temperature range. We distinguish two different types of behavior between the sets of multilayers. In the samples deposited on MgO (by MBE and Sputtering) the ideal resistivity and its temperature derivative decrease with increasing  $t_{\text{Cr}}$  thickness. On the other hand, in the samples deposited on Si,  $\rho_i$  and  $d\rho/dT$  initially increase with  $t_{\text{Cr}}$  for  $t_{\text{Cr}} \leq 40\text{\AA}$ , and then decrease as the Cr layer thickness grows.

In principle in the temperature range reported here, electron-phonon (s-s), electron-magnon and phonon-assisted interband (s-d) electron scattering may be operative [3,4]. Electron-magnon scattering gives a  $T^2$  dependence in  $\rho$  [4], leading to a linear temperature dependence in  $d\rho/dT$ . To reduce this contribution to the ideal electrical resistivity we have

performed the electrical resistivity measurements with a saturating magnetic field of 7.5kOe, and as shown in figure 1c) and 1d) this linear term is not the main contribution to  $d\rho/dT$  for  $T < 100K$ .

In fact, for  $15K < T < 50K$  we observe a  $T^2$  dependence in  $d\rho/dT$  for all the Fe/Cr multilayers studied, as shown in figure 2a) and 2b). This means that  $\rho_i = \beta T^3$ , suggesting the dominance of phonon assisted interband s-d electron scattering [4] in that temperature range ( $\rho_{sd} \propto$  lattice specific heat  $\propto (T/\Theta)^3$  when  $T$  is considerably less than the Debye temperature  $\Theta$ ;  $\Theta \sim 420K$  in our case). From the linear fits shown in figure 2a) and 2b) we have determined  $\beta$  for all the measured  $Fe_{30\text{\AA}}Cr_{t\text{\AA}}$  multilayers.

For  $T > 50K$  the exponent  $n$  (in  $\rho \sim T^n$ ) progressively decreases, reflecting the expected decay of lattice quantization effects and leading to the classical linear increase of the resistivity with temperature ( $n \cong 1$  for  $T > \sim 150K$  in our case).

By plotting the intrinsic resistivity  $\rho_{,i}^k$  for different samples  $k$ , at any temperature, as a function of the corresponding  $\beta_k$  coefficient (obtained from the low temperature fits referred above), we find good straight lines through the origin in spite of the different magnitude and behavior of  $\rho$  in each sample. These lines contain the experimental points from all the samples studied here, at that particular temperature (Fig. 2c). This means that the intrinsic resistivity can be written as:

$$\rho_{,i}^k(T) = \beta_k \cdot f(T)$$

where  $f(T)$  is a universal function of temperature, going as  $T^3$  at low temperatures and as  $T$  at high temperatures. This suggests the dominance of a single physical mechanism in the electrical resistivity over the whole temperature range,  $\sim 15-300K$ , for all the Fe/Cr multilayers studied. This mechanism is here attributed to phonon assisted interband s-d electron scattering. We have also plotted  $\rho_{,i}^k$  versus  $\beta$  for electrical resistivity measurements performed in these samples without an applied magnetic field. The slope of the linear fits to the  $\rho_{,i}^k$  versus  $\beta_k$  shown in figure 2 is slightly higher for samples measured at saturation field than the corresponding one in the samples measured at zero magnetic field. This means that the function  $f(T)$  is slightly different in both cases, which arises from the temperature

dependence of  $\Delta\rho=\rho(T,H=0)-\rho(T,H>H_{\text{sat}})$ . In our AF-coupled samples  $\Delta\rho$  is proportional to  $T^2$  at low temperatures, due to electron-magnon scattering, as expected for strong antiferromagnetic coupling as in Fe/Cr multilayers [5].

To simulate the observed temperature dependence of the electrical resistivity we have used a model that takes into account intraband s-s and interband s-d electron-phonon scattering. The s-s ( $\rho_{\text{ss}}$ ) term is modeled by a simple Bloch-Gruneisen equation whereas the s-d term ( $\rho_{\text{sd}}$ ) is defined like in [4]. The ideal electrical resistivity can then be simply written as:

$$\rho_i = A \left( \frac{T}{\Theta} \right)^3 \int_0^{\Theta/T} \frac{y^3}{(e^y - 1)(1 - e^{-y})} dy + B \left( \frac{T}{\Theta} \right)^5 \int_0^{\Theta/T} \frac{y^5}{(e^y - 1)(1 - e^{-y})} dy \quad (1)$$

where  $\Theta$  is the Debye temperature.

From equation (1) it is possible to determine the expected temperature dependence of the electrical resistivity in low and high temperature limits. In the low temperature limit, the term corresponding to phonon assisted interband s-d scattering, goes to zero as  $T^3$ . Since the term corresponding to intraband s-s scattering goes to zero as  $T^5$  it becomes negligible for temperatures lower than  $\sim 50\text{K}$  remaining only the contribution from phonon assisted interband s-d scattering as observed experimentally.

On the other hand, in the high temperature limit, equation (1) gives:

$$\rho_i \cong \frac{2A + B}{4\Theta} \times T \quad (2)$$

This indicates that the electrical resistivity should behave linearly with temperature as was observed experimentally in our samples. The model then reproduces the experimentally observed  $\rho_i$  temperature dependence, in these limits.

By using equation (1), the temperature dependence of the derivatives of  $\rho_{\text{sd}}/A$  and  $\rho_{\text{ss}}/B$  were calculated and then fitted to the experimental curves of  $d\rho/dT$  measured with an applied saturation magnetic field ( $H > H_s$ ). The Debye temperature was determined to be  $\Theta = 420\text{K}$  (near the average between  $\Theta_{\text{Fe}}$  e  $\Theta_{\text{Cr}}$ ). This value was fixed during the calculations, since it was observed to be almost invariant with Cr layer thickness.

Figure 3 shows the corresponding fits to the  $d\rho/dT$  curves of  $\text{Si}/[\text{Fe}_{30\text{\AA}}/\text{Cr}_{16\text{\AA}}]\times 10$  and  $\text{MgO}/[\text{Fe}_{30\text{\AA}}/\text{Cr}_{19\text{\AA}}]\times 10$  indicating that the experimental curves are well reproduced by this model, in the whole temperature range. From these fittings, A and B were determined and the corresponding  $\rho_{ss}$  and  $\rho_{sd}$  were obtained for all the samples studied. It was observed that electron phonon with interband s-d scattering amounts to  $\sim 75\%$  of the electrical resistivity at room temperature. As the temperature drops, the relative contribution from electron-phonon scattering with interband s-d transitions increases, since  $\rho_{ss}$  decreases faster than  $\rho_{sd}$  as the temperature drops. This indicates the dominance of phonon assisted interband s-d electron scattering in the whole temperature range, as remarked earlier.

According to equation (1) the ideal electrical resistivity can be written as  $\rho_i = A \times f_1(T) + B \times f_2(T)$  where  $f_1$  and  $f_2$  are functions only of the temperature. Since A and B are sample dependent constants it is not expected a priori that exists any relation between them independent of each particular multilayer.

By plotting B versus A we find that each point from all the multilayers falls in a straight line indicating that B is proportional to A, as shown in figure 4. The slope of this line is  $\sim 0.5$  so that  $B = A/2$  for all the multilayers. This means that equation (1) can be written as:

$$\rho_i = A \left( \frac{T}{\Theta} \right)^3 \left[ \int_0^{\Theta/T} \frac{y^3}{(e^y - 1)(1 - e^{-y})} dy + \frac{1}{2} \left( \frac{T}{\Theta} \right)^2 \int_0^{\Theta/T} \frac{y^5}{(e^y - 1)(1 - e^{-y})} dy \right] \quad (3)$$

The simulated resistivity thus predicts that  $\rho_i = \beta f(T)$  ( $\rho_i = \rho - \rho_0$ ) where  $f(T)$  a function only of the temperature and  $\beta$  is a sample dependent constant, as observed experimentally (figure 2d).

In conclusion, the simple model here presented including phonon assisted intraband s-s and interband s-d electron scattering accounts well with the main features observed in the temperature dependence of electrical resistivity and its temperature derivative, in the range  $\sim 15\text{-}300\text{K}$  and under saturation magnetic field. Since s-s and s-d electron phonon scattering contributions are almost independent of the applied field, the extension of this model to zero magnetic field only needs an extra term to account the electron-magnon scattering contribution to the electric resistivity.

## Figure captions

Figure 1: Temperature dependence of the ideal electrical resistivity (1a and 1b) and its temperature derivative (1c and 1d) measured in  $\text{Fe}_{30\text{\AA}}/\text{Cr}_{t\text{\AA}}$  multilayers deposited by sputtering on MgO and Si.

Figure 2: Linear fits to the temperature derivative of the electrical resistivity *versus*  $T^2$  measured at  $H > H_{\text{sat}}$  in  $\text{Fe}_{30\text{\AA}}/\text{Cr}_{t\text{\AA}}$  multilayers deposited by sputtering on a) MgO and b) Si, for  $T < 50\text{K}$ . Also shown is the ideal resistivity measured at c) saturation and d) zero magnetic field *versus*  $\beta$  for the Fe/Cr multilayers studied.

Figure 3: Temperature dependence of the electrical resistivity measured in  $\text{Si}/[\text{Fe}_{30\text{\AA}}/\text{Cr}_{16\text{\AA}}] \times 10$  and  $\text{MgO}/[\text{Fe}_{30\text{\AA}}/\text{Cr}_{19\text{\AA}}] \times 10$  multilayers. Also shown are the corresponding curves fitted with the model described in the text.

Figure 4: Plot of B *versus* A using the fitted values obtained with equation (1), for all the multilayers studied. The graph shows the existence of a linear relation between them, with slope  $\sim 0.5$ .

## References

- [1] - P.M. Levy, *Solid State Physics*, edited by H. Ehrenreich and Turnbull, Academic, New York, **47**, 367, (1994)
- [2] - J.M. Colino, I.K. Schuller, R. Schad, C.D. Potter, P. Belien, G. Verbanck, V.V. Moshchalkov and Bruynseraede Y.; *Phys. Rev. B*, **53**, 766 (1996)
- [3] - Duvail J.L, Fert A., Pereira L.G., Lottis D.K., *J. Appl. Phys.*, **75**, (10), 7070 (1994)
- [4] - Mattson J.E., Brubaker M.E., Sowers C.H., Conover M., Qiu Z., and Bader S.D.; *Phys. Rev. B*, **44**, 9378, (1991); B. Loegel and F. Gautier, *J. Phys. Chem. Solids*, **32**, 2723 (1971)
- [5] - Y. Saito, K. Inomata, S. Uji, T. Terashima, and H. Aoki; *J. Phys. Soc. Japan*, **63**, 1263 (1994)

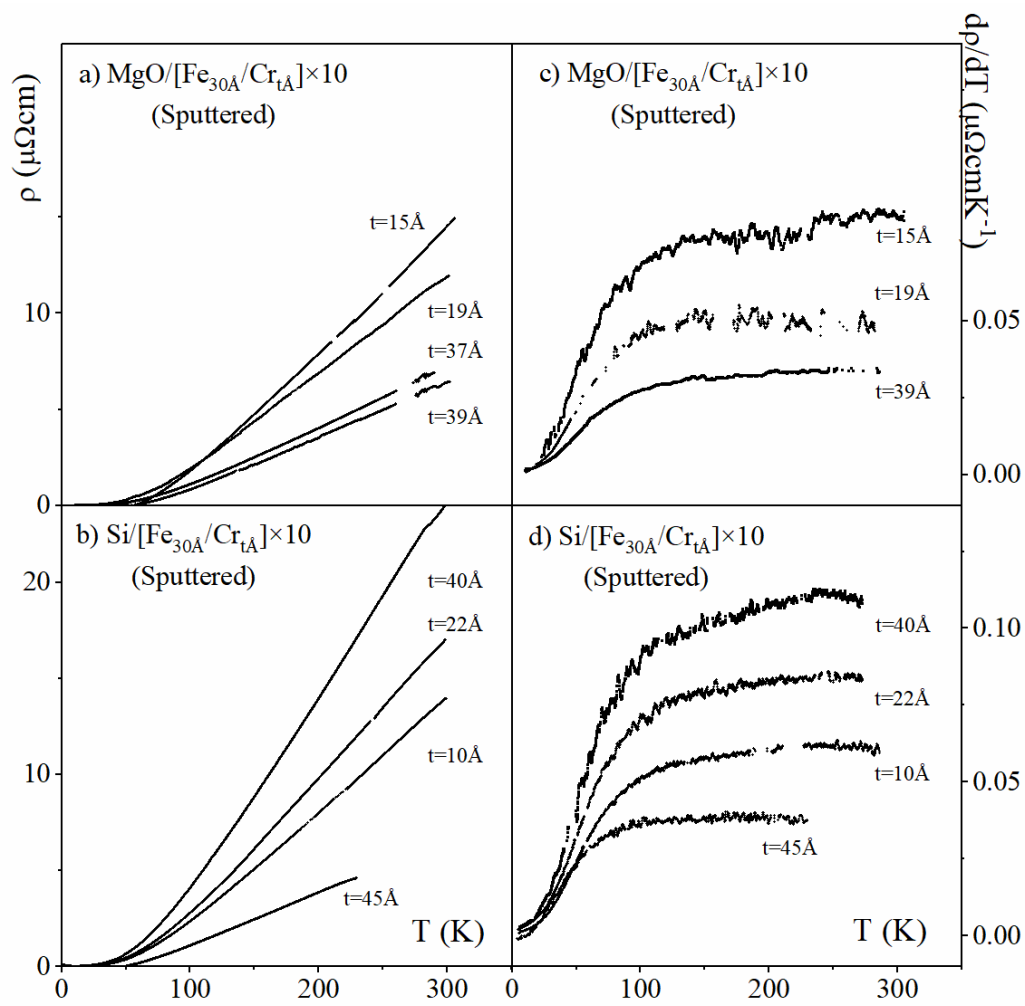


Figure 1 - B.G. Almeida



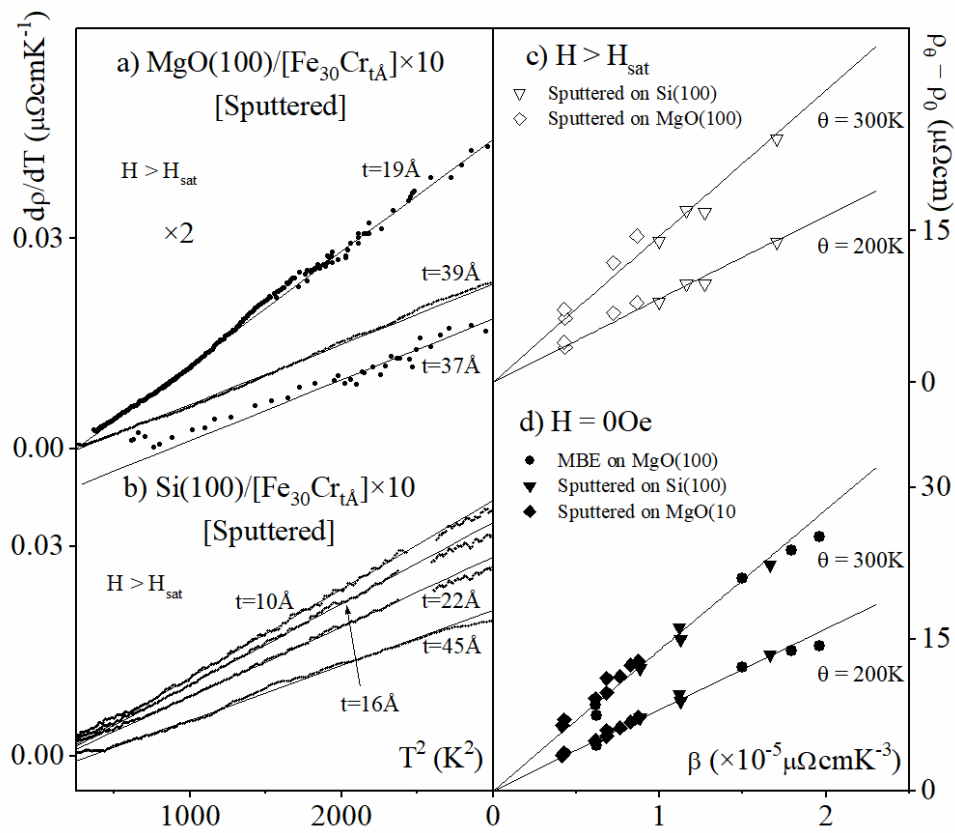


Figure 2 - B.G. Almeida

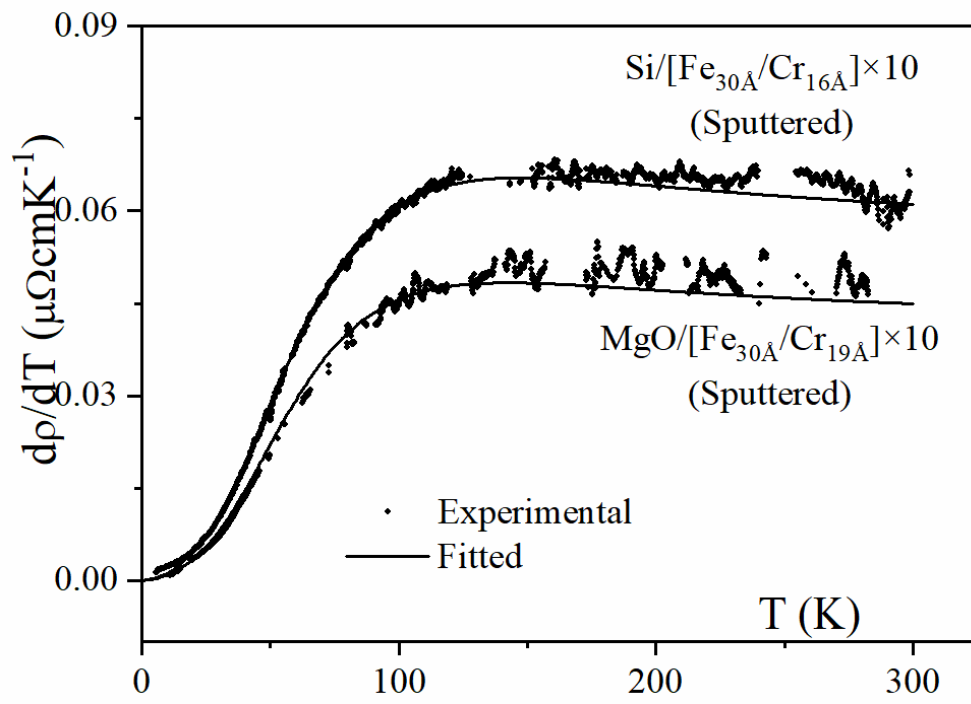


Figure 3 - B.G. Almeida

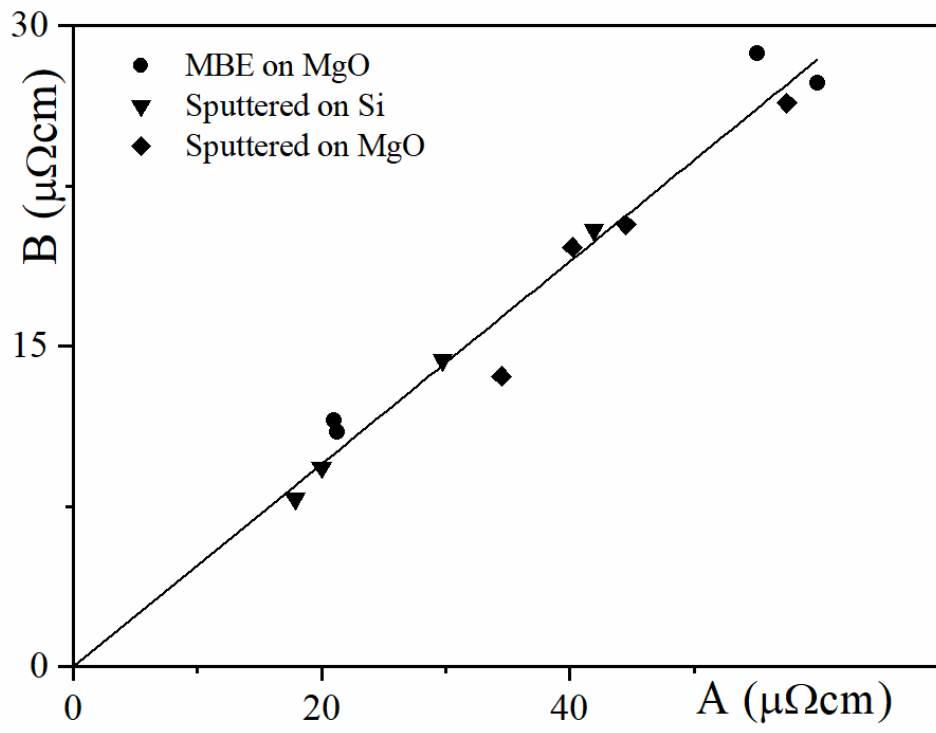


Figure 4 - B.G. Almeida